Biosensors and Bioelectronics 81 (2016) 61–67

Contents lists available at ScienceDirect

Biosensors and Bioelectronics

journal homepage: www.elsevier.com/locate/bios

Nanoporous Au-based chronocoulometric aptasensor for amplified detection of Pb^{2+} using DNAzyme modified with Au nanoparticles

Chen Zhang [a,b], Cui Lai [a,b], Guangming Zeng [a,b,*], Danlian Huang [a,b,*], Lin Tang [a,b], Chunping Yang [a,b], Yaoyu Zhou [a,b], Lei Qin [a,b], Min Cheng [a,b]

[a] College of Environmental Science and Engineering, Hunan University, Changsha 410082, PR China
[b] Key Laboratory of Environmental Biology and Pollution Control, Hunan University, Ministry of Education, Changsha 410082, PR China

ARTICLE INFO

Article history:
Received 26 December 2015
Received in revised form
14 February 2016
Accepted 19 February 2016
Available online 21 February 2016

Keywords:
Pb^{2+}
Nanoporous Au
Au nanoparticles
Aptasensor
Amplification

ABSTRACT

The authors herein described an amplified detection strategy employing nanoporous Au (NPG) and gold nanoparticles (AuNPs) to detect Pb^{2+} ions in aqueous solution. The thiol modified Pb^{2+}-specific DNAzyme was self-assembled onto the surface of the NPG modified electrode for hybridizing with the AuNPs labeled oligonucleotide and for forming the DNA double helix structure. Electrochemical signal, redox charge of hexaammineruthenium(III) chloride (RuHex), was measured by chronocoulometry. Taking advantage of amplification effects of the NPG electrode for increasing the reaction sites of capture probe and DNA-AuNPs complexes for bringing about the adsorption of large numbers of RuHex molecules, this electrochemical sensor could detect Pb^{2+} quantitatively, in the range of 0.05–100 nM, with a limit of detection as low as 0.012 nM. Selectivity measurements revealed that the sensor was specific for Pb^{2+} even with interference by high concentrations of other metal ions. This sensor was also used to detect Pb^{2+} ions from samples of tap water, river water, and landfill leachate samples spiked with Pb^{2+} ions, and the results showed good agreement with the found values determined by an atomic fluorescence spectrometer. This simple aptasensor represented a promising potential for on-site detecting Pb^{2+} in drinking water.

1. Introduction

In 2003, the hazardous levels of lead contamination detected in Washington D.C. drinking water aroused people's extensive attention (Chen et al., 2005; Renner, 2004; Zeng et al., 2013a, 2013b). Exposure to trace amount of lead can cause neurological, cardiovascular, reproductive, and developmental disorders (Fan et al. 2008; Huang et al., 2008; Jain et al., 2006; Marbella et al., 2009). The maximum contamination level (MCL) for lead in drinking water is defined by the U.S. Environmental Protection Agency (EPA) to be 72 nM (even lower than 72 nM of lead is associated with children's neuro-developmental deficits) (Yang et al., 2010). Hence, it is essential to develop sensors for ultrasensitive detection of Pb^{2+}.

Analytical methods [e.g., atomic absorption spectrometry (AAS), inductively coupled plasma optical emission spectrometry (ICP-OES), and inductively coupled plasma mass spectrometry (ICP-MS)] are the standard techniques utilized for Pb^{2+} determination (Arduini et al., 2010; Liang and Sang, 2008; Quintana et al., 2012). These methods are very sensitive, selective, accurate and can be used to detect different kinds of metal ions but require expensive and complex equipment, materials and include time consuming extraction steps to eliminate the excipients, contaminants and interfering ions (Yola et al., 2012). In addition, the analysis must be performed in a specialized laboratory by skilled personnel. Electrochemical techniques have attracted considerable interest due to their remarkable sensitivity, low cost, portability and inherent simplicity (Ge et al., 2014; Tang et al., 2008).

In developing highly sensitive electrochemical sensors, amplified detection strategy is the central research topic. Various signal amplification strategies, such as the utilization of nanomaterials as electrode materials to construct sensing platforms and carriers for increasing the upload of electrochemical tags, the integration of enzyme-assisted signal amplification processes, and the employment of new labels and so on, have been developed (Dreaden et al., 2012; Huang et al., 2013b; Saha et al., 2012; Shen et al., 2008; Wu et al., 2014). Particularly, great attention has been paid to different nanomaterials, such as metal nanoparticles (NPs), quantum dots (QDs), magnetic nanoparticles (MNPs), carbon-based nanomaterials and polymeric NPs (Aragay et al., 2012; Chen and

* Corresponding authors at: College of Environmental Science and Engineering, Hunan University, Changsha 410082, PR China.
E-mail addresses: zgming@hnu.edu.cn (G. Zeng), huangdanlian@hnu.edu.cn (D. Huang).

http://dx.doi.org/10.1016/j.bios.2016.02.053
0956-5663/

Chatterjee, 2013; Huang et al., 2013a; Xu et al., 2012; Zhang et al., 2007; Zhou et al., 2016a, 2014a). Recently, nanoporous gold (NPG) has attracted considerable attention due to its high surface-to-volume reaction, excellent conductivity, stability and biocompatibility (Zhang et al., 2014b). The use of NPG electrode can increase the electrochemical signals and lower the detection limits by the enhancement of electron transfer on the electrode surface and the enlargement of the surface area of the substrate electrode. For the preparation of nanoporous electrodes, dealloying method, by which Ag was dissoluted from Au/Ag alloy in nitric acid, to make controllable three-dimensional nanoporous metal films, has been reported (Ding and Erlebacher, 2003; Erlebacher et al., 2001; Zhang and Li, 2012). The free-standing NPG films yield a robust and sensitive current response to reactions such as CO and glucose oxidation (Xu et al., 2007; Zhang and Li, 2012). Furthermore, oligonucleotide-functionalized gold nanoparticles (AuNPs) have been employed as amplifying tags for biosensing protocols due to their unique properties (Brakmann, 2004; Shen et al., 2008). Plaxco and co-workers have developed an electrochemical sensor for Pb^{2+}, taking advantage of catalytic reactions of a deoxyribozyme (DNAzyme) and using DNA-Au bio-bar codes to achieve signal enhancement, which achieved nanomolar sensitivity (Xiao et al., 2006). Yang et al. (2010) also developed an electrochemical sensor for detection of Pb^{2+} using DNAzyme functionalized gold AuNPs as a means of amplification, enabling the detection limit to be 0.028 nM. Zeng and our team developed a sensitive electrochemical Pb^{2+} sensor using a carboxylic acid group functionalized multi-walled carbon nanotubes/AuNPs-modified electrode and taking advantage of Pb^{2+}-induced G-rich DNA conformation, with a limit of detection as low as 4.3×10^{-6} nM (Zhu et al., 2014). However, the reported electrochemical lead detection methods require complex and multistep protocols. Thus it is necessary to develop a simple and efficient sensor for the detection of lead. Here we propose a simpler electrochemical approach based on the NPG electrode and highly specific, metal-induced activation of a lead-requiring DNAzyme.

This work has assessed the characteristics of NPG and AuNPs, and enabled us to construct a highly sensitive electrochemical sensor for amplified detection of Pb^{2+}. Taking advantaging of NPG electrode as a solid support for the immobilization of probe DNA and using a specially designed DNAzyme-AuNPs system to achieve signal enhancement were investigated. Compared with the common Pb^{2+} sensor, the proposed sensor is based on the amount of surface confined DNA switch, which is independent of the unique structures of DNA such as the G-quadruplex (Zhu et al., 2014), hairpin (Baker et al., 2006), or stem-loop (Ke et al., 2003). Moreover, the amplification system avoids the time-consuming synthetic procedures, thereby achieving a sensitive, rapid, and simple chronocoulometric aptasensor.

2. Materials and methods

2.1. Materials and apparatus

Au-Ag alloy foils (100 nm in thickness, 50:50, w/w) were kindly provided by Prof. Ding, Y., Shandong University, Jinan 250100, P. R. China. The synthesized oligonucleotides were purchased from Sangon Biotech. Co., Ltd. (Shanghai, China). The sequences were as follows: Probe 1 (P1): 5′-SH-$(CH_2)_6$-TTTCATCTCTTCTCC-GAGCCGGTCGAAATAGTGAGT-3′; Probe 2 (P2): 5′-SH-$(CH_2)_6$-ACT-CACTATArGGAAGAGATG-3′. P1 is the Pb^{2+}-specific DNAzyme and P2 is the substrate oligonucleotide. Tris (2-carboxyethyl) phosphinehydrochloride (TCEP), hexaammineruthenium(III) chloride (RuHex), and 6-mercaptohexanol (MCH) were purchased from Sigma-Aldrich Chemical Co. All other chemicals were of analytical grade and were used without further purification. Ultrapure water (18.2 MΩ cm) was used throughout the experiments. The buffers involved in this work are as follows: 10 mM Tris-acetate buffer (pH 8.0), 500 mM acetate buffer (pH 5.2), and Tris-EDTA buffer (TE, 10 mM Tris–HCl and 1 mM EDTA, pH 8.0).

Electrochemical measurements were carried out on a CHI760D electrochemistry system (Chenhua Instrument, China). The three-electrode system used in this work consisted of a glass carbon electrode (GCE, 3 mm in diameter) as working electrode, a saturated calomel electrode (SCE) as reference electrode and a Pt foil auxiliary electrode. The microstructure of NPG electrode surface was observed by a JSM-6700F field emission scanning electron microscope (JEOL Ltd., Japan). The surface area of NPG was measured with Quantachrome NOVA 2000e using the BET method (Quantachrome Instrument, USA). The transmission electron microscopy (TEM) image of AuNPs was measured with a JEOL JEM-3010 transmission electron microscopy (JEOL Ltd., Japan). UV–vis absorption spectra were recorded using a Shimadzu UV spectrophotometer (UV-2550, Japan). All work was performed at room temperature (25 °C) unless otherwise mentioned.

2.2. Sensor fabrication

The GCE was first polished in the aqueous slurry of alumina and rinsed with deionized water. Residual alumina particles were thoroughly removed by sonicating electrodes in ethanol and deionized water for 5 min, respectively. Then the GCE was sonicated in “piranha solution” (H_2SO_4: 30% H_2O_2=3:1, V/V), and rinsed with ultrapure water. After being dried with nitrogen, the NPG foil (prepared by selective dissolution of Ag from Ag/Au) was carefully coated onto a pretreated GCE via physical adsorption after being washed with ultrapure water to neutral pH (Ding et al., 2004; Hu et al., 2008; Zhang et al., 2014b). The freshly prepared NPG electrode was incubated in a solution composed of 1 μM P1, 10 mM Tris-acetate buffer (pH 8.0), and 1 mM TCEP (which is included to reduce disulfide bonded oligomers) (Yang et al., 2010) for 12 h. The P1 modified NPG electrode was then passivated with 1 mM MCH for 2 h followed by washing with 10 mM Tris-acetate buffer (pH 8.0) to reduce nonspecific adsorption of P1 and to obtain a well aligned DNA monolayer (Levicky et al., 1998).

2.3. Preparation of DNA probe functionalized AuNPs

AuNPs were prepared by citrate reduction of $HAuCl_4$ according to literature (Liu and Lu, 2006; Zhang et al., 2014a) with some modification. Briefly, 10 mL of 38.8 mM trisodium citrate was rapidly added to a boiled 100 mL of 1 mM $HAuCl_4$ solution with vigorous stirring for 15 min in a 250 mL round-bottom flask equipped with a condenser. The color changed from pale yellow to wine red in 1 min, indicating the formation of AuNPs. The solution was cooled to room temperature (23–25 °C) under stirring. The average diameter of such prepared AuNPs was ~15 nm measured by zetasizer nano Zs and TEM (see Fig. S5). According to Beer's law using UV–vis spectroscopy based on the extinction coefficient of $2.7\times10^8\ M^{-1}\ cm^{-1}$ at λ=520 nm for 13 nm particles, the concentration of the AuNPs was ~10 nM (Haiss et al., 2007; Huang et al., 2013b).

AuNPs is readily functionalized with thiolated P2 via the well-known gold–sulfur chemistry (Taton et al., 2000). Conjugates of oligonucleotide P2-AuNPs were synthesized following the protocol with a slight modification (Liu and Lu, 2006). In brief, 9 μL of 10 μM thiol-modified P2 was activated with 1 μL of 0.5 M acetate buffer (pH 5.2) and 1.5 μL of 10 mM TCEP for 1 h and added to 1.0 mL of AuNPs, storing in a drawer for at least 16 h (magnetic stirring may also be applied to facilitate the reaction). The P2-AuNPs conjugate was aged in 100 mM NaCl and 10 mM Tris-

acetate buffer (pH 8.0) for at least another day. Most of the free P2 was removed by two centrifugations: firstly, the P2-AuNPs solution was centrifuged at 15000 rpm for 20 min and then the red nanoparticle precipitate was dispersed in 200 μL of buffer containing 100 mM NaCl and 10 mM Tris-acetate (pH 8.0); secondly, recentrifuged and dispersed in 500 μL of buffer containing 300 mM NaCl and 10 mM Tris-acetate (pH 8.0). The solution was stored at 4 °C.

2.4. Assembly of DNA-AuNPs on NPG electrode

For the hybridization reaction, P1 modified NPG electrode was immersed into the P2-AuNPs solution for 2 h at 37 °C. Temperature stability was accomplished by the temperature-controlled thermostat. Finally, the electrode was immersed in buffer (10 mM Tris-acetate, pH 8.0) for 5 min to reduce the nonspecific adsorption of P2-AuNPs.

2.5. Detection and calculation

The modified electrode reacted with various concentrations of Pb^{2+} in buffers (10 mM Tris-acetate, 100 mM NaCl, pH 8.0) for 40 min at 37 °C. Then the electrode was immersed in buffer solution (10 mM Tris-acetate, pH 8.0) for 5 min to remove the nonspecific adsorption of P2-AuNPs. Chronocoulometry (CC) was performed in 5 mL of 10 mM Tris-acetate solution (pH 8.0) containing 50 μM RuHex. The experiment of CC started at a potential of 0 V (Initial E) at which there was no electrolysis. The potential was then changed instantaneously to a value of 0.7 V (Final E) that led to the reaction of RuHex in solution and was held at 0.7 V for 250 ms. Cyclic voltammetry (CV) measurements were carried out at the potential range of −0.3 to 0.8 V at scan rate of 50 mV s^{-1}. Electrochemical impedance spectra (EIS) was performed in 0.1 M PBS (pH 7.4) containing 5 mM $[Fe(CN)_6]^{3-/4-}$ (1:1) and 10 mM KCl in the frequency range from 0.1 Hz to 100 kHz with 5 mV as the amplitude at a polarization potential of 0.18 V. Optimization experiments, detection limit and selectivity tests were next performed. In all optimization experiments, 1.0 nM Pb^{2+} was used and selectivity measurement, 10 nM Pb^{2+} was used.

2.6. Environmental samples analysis

Three different environmental samples, tap water, river water, and landfill leachate sample were used in this study. Tap water was derived from Changsha Running-water Company, China. River water was taken from Dongting Lake, China. And landfill leachate was obtained from municipal solid waste landfills in Changsha, China. They were centrifuged at 10000 rpm for 5 min and filtered to remove the suspension and solid impurities. The pH of the sample solutions was then adjusted to 8.2. The solutions were next spiked with different concentrations of Pb^{2+}. Detection of Pb^{2+} was then conducted using the developed biosensor. Meanwhile, the same samples were filtrated via the 0.2-μm polycarbonate filter and analyzed by atomic fluorescence spectrometry (AFS) as a standard detection method for validation the sensor.

3. Results and discussion

3.1. Experimental principle and sensing scheme

In the present study based on the Pb^{2+}-specific DNAzyme ("8–17" DNAzyme), the authors fabricated an amplified electrochemical sensor for highly sensitive and selective detection of Pb^{2+}. The sensing strategy is shown in Scheme 1. NPG, prepared by selective dissolution of Ag/Au alloy with controlled size and spatial arrangement of pores, was coated onto a pretreated GCE via physical adsorption, followed by the self-assembly of the thiol modified oligonucleotide capture probe, P1. After treatment with MCH for eliminating nonspecific binding on electrode surface and also for keeping DNAzyme activity, the GCE-NPG-P1 was allowed to interact with the P2-AuNPs complexes and the double stranded DNA was obtained by hybridization of P1 with its partially complementary P2. When the as-prepared GCE-NPG-P1-P2-AuNPs was incubated with the solution containing Pb^{2+}, the catalytic strand P1 carried out catalytic reactions to give hydrolytic cleavage of the substrate strand P2 at the scissile rA (Wang et al., 2008; Yang et al., 2010). Chronocoulometry was initially employed to

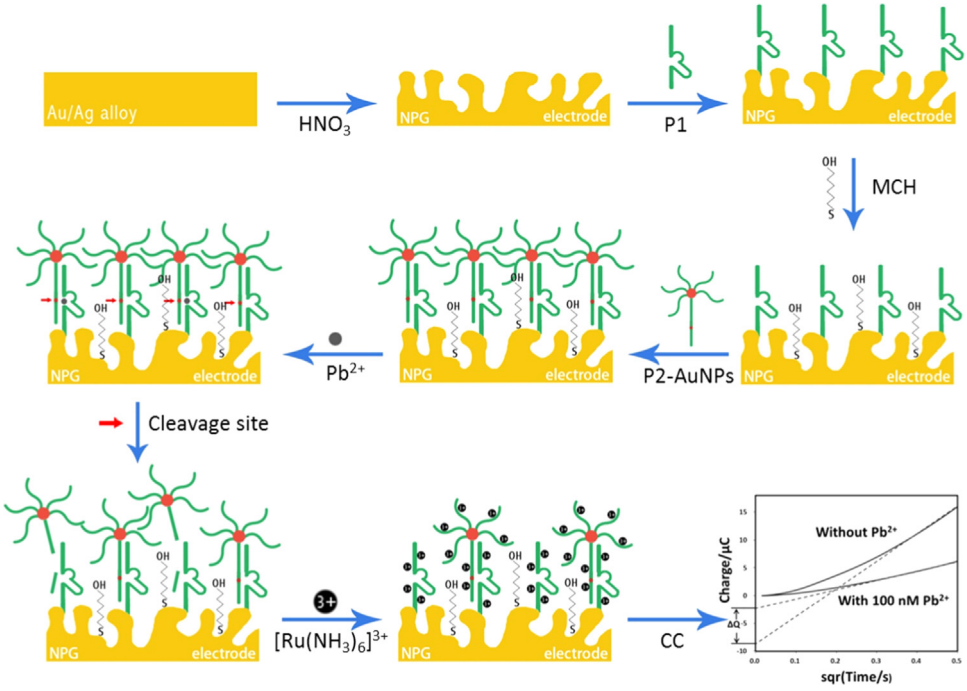

Scheme 1. Schematic illustration of the aptasensor preparation and the proposed mechanism for the Pb^{2+} detection.

quantify DNA surface density via measuring redox charge (Q) of RuHex at surfaces, and it was used to quantify immobilized DNA recently. Chronocoulometry involves measurement of the charge vs. time response to an applied potential step waveform. The shape of the resulting chronocoulogram can be understood by considering the concentration gradients in the solution adjacent to the electrode surface. Chronocoulometry, which has been proved to be a more accurate electrochemical technique than cyclic voltammetry to quantify the amount of DNA (Lao et al., 2005), was selected to measure the Pb^{2+} concentration, because the chronocoulometric signal is linearly proportional to the amount of DNA, which depends on the concentration of Pb^{2+}. Taking advantage of amplification effects of the NPG electrode for increasing the reaction sites of capture probe (P1) and DNA-AuNPs complexes for providing a great number of sites for adsorption of RuHex molecules, this electrochemical sensor design would display a satisfactory detection capability in theory.

3.2. Characterization of the NPG electrode

Apart from excellent biocompatibility, Au-based 3D porous structure is a suitable candidate for fabricating aptasensors, because its large surface area can realize significantly amplified detection (Feng et al., 2011; Zhang et al., 2013). The pore/ligament size of NPG is controllable by varying etching time and temperature, or the initial alloy ingredient (Zhang et al., 2014b). As shown in Fig. 1A, dealloying Ag/Au foil at 25 °C for 2 h resulted in a nanoporous structure. Moreover, the dynamic changes of the layer by layer were characterized by field emission scanning electron microscope (see Fig. S1). Compared with NPG (Fig. S1B), the P1 modified NPG (Fig. S1C) was more blurred due to the poor electrical conductivity of oligonucleotides, and the pore size became slightly smaller. After assembly of P2-AuNPs, the pore size of P1-P2-AuNPs modified NPG electrode was getting smaller than P1 modified NPG and even a slight blocking phenomenon was observed (Fig. S1D). The used Au–Ag alloy foil was ca. 100 nm thick, and the gold loading of the prepared NPG film was ca. 0.1 mg cm^{-2}. The real surface area of NPG was estimated to be ca. 10.8 m^2 g^{-1} using the BET method. The NPG electrode had a total active surface of 211.9 mm^2, while the corresponding bare GCE electrode was 19.6 mm^2. The significant enhancement of 10.8-fold was obtained, representing a much larger surface area and more reaction sites of the Au-based 3D porous electrode (Qiu et al., 2009). The number of pore layers was ca. 3.0, and the theoretical value was obtained via the equation of relative surface enhancement between a flat and a nanoporous electrode, according to fundamental geometric considerations, supposing a close-packed structure (Szamocki et al., 2007):

$$f = n\pi(4/3)^{1/2} \quad (1)$$

With f being the enhancement factor and n the number of pore layers.

Cyclic voltammetry (CV) was carried out to test the property of the modified electrode. Fig. 1B was the electrochemical responses of $Fe(CN)_6^{3-}/Fe(CN)_6^{4-}$ at the NPG/GCE, AuNPs/GCE and polished GCE. It showed that the peak current at NPG/GCE was ca. 2.2-fold higher than that at GCE, and even 1.6-fold higher than that at AuNPs/GCE (widely used strategies as it offers the advantages of convenience and wide application in electrocatalysis and electroanalysis) (Wu et al., 2014) due to the larger active surface area of NPG/GCE. However, the peak current increase was not as significant as that expected on the basis of the increment in surface area. This observed phenomenon might be caused by fast electron transfer of the redox couple at the outermost layer, and the inner porous surface might be ineffective if the reactant concentrations

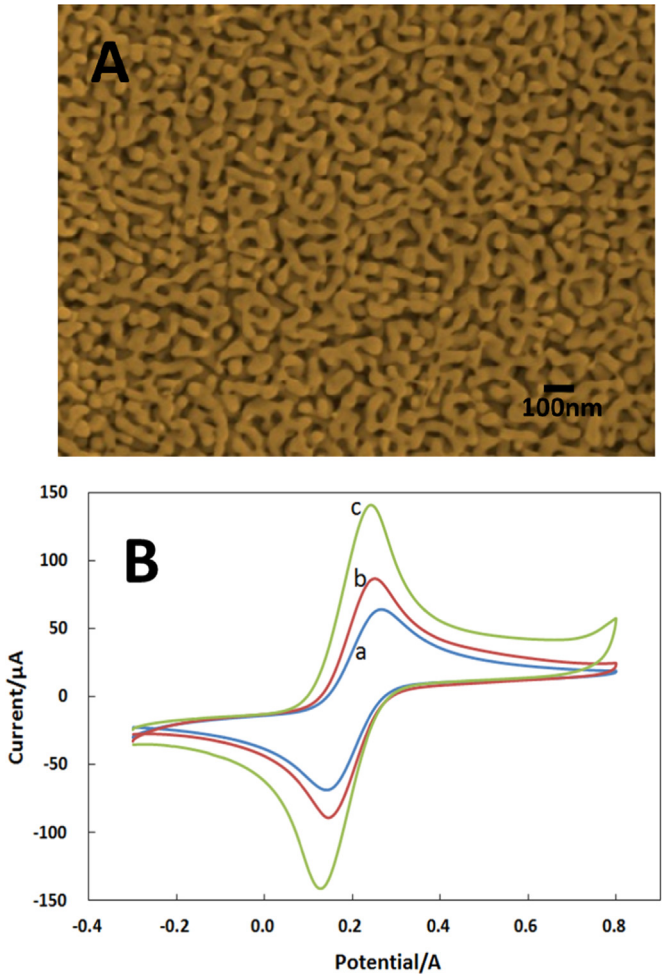

Fig. 1. Field emission scanning electron microscope image of the NPG with a pore size of ~40 nm (A); cyclic voltammograms (B) of bare GCE (a), AuNPs/GCE (b), NPG/GCE (c) modified electrode in 10 mM KCl solution containing 5.0 mM ferricyanide at a scan rate of 50 mV s^{-1}.

from the bulk solution dropped down to zero at the outer surface layer (Park et al., 2003; Qiu et al., 2009). The reproducibility of NPG modified electrodes was also studied, and the results indicated that the NPG modified electrodes exhibited excellent reproducibility (see Fig. S2).

3.3. Characterization of the NPG-based biosensor

Electrochemical impedance spectroscopy (EIS) was applied to characterize the layer-by-layer assembling process of the NPG-based aptasensor. The semicircle diameter represented the electron-transfer resistance in EIS. Fig. 2 illustrated the Nyquist plot of impedance for the stepwise modification process with the NPG/GCE electrode in a 5 mM $Fe(CN)_6^{3-}/Fe(CN)_6^{4-}$ phosphate buffer containing 10 mM KCl at an open circuit potential with the frequency varied from 0.01 Hz to 100 kHz. Moreover, the interface can be modeled by an equivalent circuit. This equivalent circuit included the electron-transfer resistance (R_{CT}), the warburg impedance (Z_w), the ohmic resistance of the electrolyte (R_s), and interfacial capacitance (C_{dl}). EIS includes a semicircular part and a linear part. The semicircle diameter could represent the electron–transfer resistance, R_{CT}, which dominates the electron transfer kinetics of the redox probe at the electrode interface. Meanwhile, the linear part at lower frequencies corresponds to the diffusion process. Besides, the interface could be modeled by an equivalent circuit by the method, which was described in our previously work

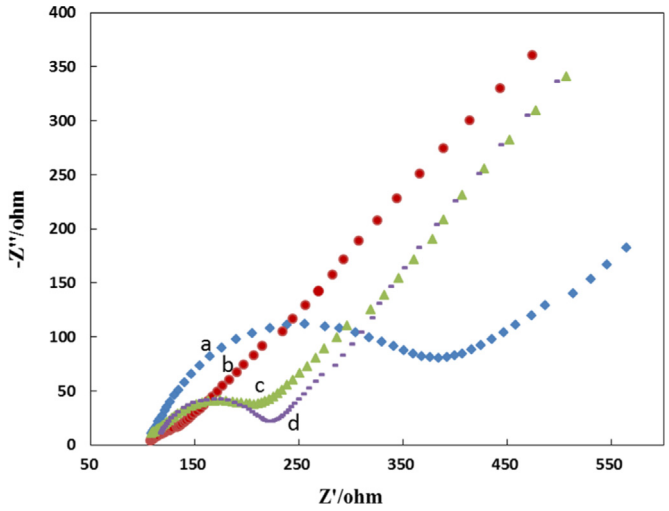

Fig. 2. Electrochemical impedance spectra (Nyquist plots) of bare GCE (a), NPG/GCE (b), P1/NPG/GCE (c), MCH/P1/NPG/GCE and (d) with frequency range from 0.01 Hz to 10^5 Hz.

(Zhou et al., 2014b, 2016b). As seen in Fig. S4, the good agreement between the measured data and the fitting curve indicated that this equivalent circuit (see Fig. S3A) was suitable and meaningful for this electrochemical system. Therefore, this equivalent circuit was used to fit the impedance spectroscopy data and extract the values of the Equivalent Circuit Elements (Table S1). The R_{CT} value of bare GCE electrode was about 403 Ω (curve a). With the modification of NPG, an almost straight line was observed and the R_{CT} value was about 15 Ω, indicating an increase in the electron transfer ability (curve b). After being self-assembled with negatively charged P1 and MCH, the R_{CT} value increased due to the electrostatic repulsion (curve c and d). However, the R_{CT} values were still quite low after P1 immobilization and MCH modification, revealing excellent conductivity of NPG. The UV–vis spectra of the Au colloid, thiolated P2 and biofunctionalized reporter P2 with AuNPs were recorded by the spectrophotometer (see Fig. S5). The results indicated that the AuNPs has been successfully labeled on thiolated P2.

3.4. Optimization of the detection strategy

A series of experiments were performed to optimize the conditions with acceptable signal response. The effect of pH condition, the reacting time with the Pb^{2+} ions, and the influence of the concentration of RuHex on the CC charge were investigated. The effect of temperature was not considered, because it is our intention that the Pb^{2+} aptasensor will be used at room temperature, which is more suitable for application.

pH value always plays an important role in chemical reactions, especially in biochemical reactions. Fig. S6A showed the CC charge difference of the NPG-P1-P2-AuNPs modified electrode in different pH buffer solutions containing 1.0 nM of Pb^{2+} ions. The electric signal maintained a high level in the pH range of 6.5–8.0. It revealed that the aptasensor had a good ability to resist the impact of pH change and was quite suitable for real sample detection. The electric signal reached the maximum when the pH value was 8.0, indicating that the double helix structure was unzipped. Therefore, pH 8.0 was noted as the best pH level to maintain the detection in good condition. The reaction time between substrate oligonucleotide and Pb^{2+} ions directly affect the detecting result and the efficiency. The results were showed in Fig. S6B. With the increasing of reacting time, the CC charge responses had an ascent and reached maximum in the reacting time of 30 min, indicating that the reaction between substrate oligonucleotide and Pb^{2+} ions was complete. Consideration from the reaction sufficiency and detection efficiency, 30 min was selected as the optimal reaction time between substrate oligonucleotide and Pb^{2+}. For the preparation of chronocoulometric aptasensor, the immobilization of RuHex on the electrode surface was a crucial step because the density of RuHex directly affected the sensor performance. Hence, before studying the sensitivity for Pb^{2+}, the influence of the concentration of RuHex on the CC charge was investigated. As shown in Fig. S6C, it was observed that the CC charge responses increased significantly with the increasing of the RuHex concentration and saturated when the RuHex concentration reached 50 μM. Thus, 50 μM RuHex was chosen in this study.

3.5. Sensitivity for Pb^{2+}

According to the above standard procedures and under the optimized assay conditions, different concentrations of Pb^{2+} were added to the buffer and the CC was carried out for the detection. The various concentrations of Pb^{2+} were 0, 0.05, 0.1, 0.5, 1.0, 5.0, 10.0, 50.0, and 100.0 nM. The experimental results were shown in Fig. 3A, and the chronocoulometric curves converted to Anson plots by plotting charge versus $t^{1/2}$ were shown in Fig. 3B. The linear part of the Anson plot was then extrapolated back to time zero to obtain the intercept for the plot in the presence and absence of Pb^{2+}. With the increase of the Pb^{2+} concentration, the charges of RuHex decreased gradually. Even at very low concentrations of Pb^{2+}, the charge exhibited perceptible change, which indicated that Pb^{2+} could be detected with high sensitivity in this proposed aptasensor. The results indicated that charges of RuHex decreased with the increase of the concentration of Pb^{2+} ranging from 0.05 to 100 nM. In Fig. 3C, the change of the charge linear regression coefficient result was 0.9887 and the detection limit was estimated to be 0.012 nM by using 3σ (where σ is the standard deviation of the blank solution, $n=3$). The reproducibility of the aptasensor for detection of 10.0 nM Pb^{2+} was 4.28% (RSD, $n=3$). Table S2 shows that the sensitivity of the nanoporous Au-based electrochemical aptasensor is superior to other DNAzyme-based biosensors for detecting Pb^{2+} as reported previously. This proposed indirect Pb^{2+} detection method obtained a low detection limit, wide linear range, and fast response time, which can completely meet the requirement of water quality monitoring (Table S2).

3.6. Selectivity for Pb^{2+}

To evaluate the selectivity of this protocol, two control experiments were conducted. First, the difference of chronocoulometry signals for Pb^{2+} and other metal ions, including Ni^{2+}, K^{+}, Ca^{2+}, Mg^{2+}, Al^{3+}, Zn^{2+}, Fe^{3+}, Cu^{2+}, Mn^{2+}, Cr^{2+}, Cd^{2+}, and Hg^{2+}, under optimum conditions were compared. As indicated in Fig. 4, in contrast to the significant response as observed for Pb^{2+}, negligible signal change was observed upon the addition of other tested metal ions. Hence, the results showed excellent selectivity toward Pb^{2+} over other metal ions because of the specificity of Pb^{2+}-dependent DNAzyme. Second, Pb^{2+} and other metal ions were mixed to form a mixture solution as a sample for the anti-jamming capability testing of the aptasensor. The chronocoulometry signal was obviously higher than other samples without Pb^{2+}. These results indicated that the approach was not only insensitive to other metal ions but also selective toward Pb^{2+} in their presence. As noted above, the present aptasensor has excellent anti-jamming capability and outstanding selectivity.

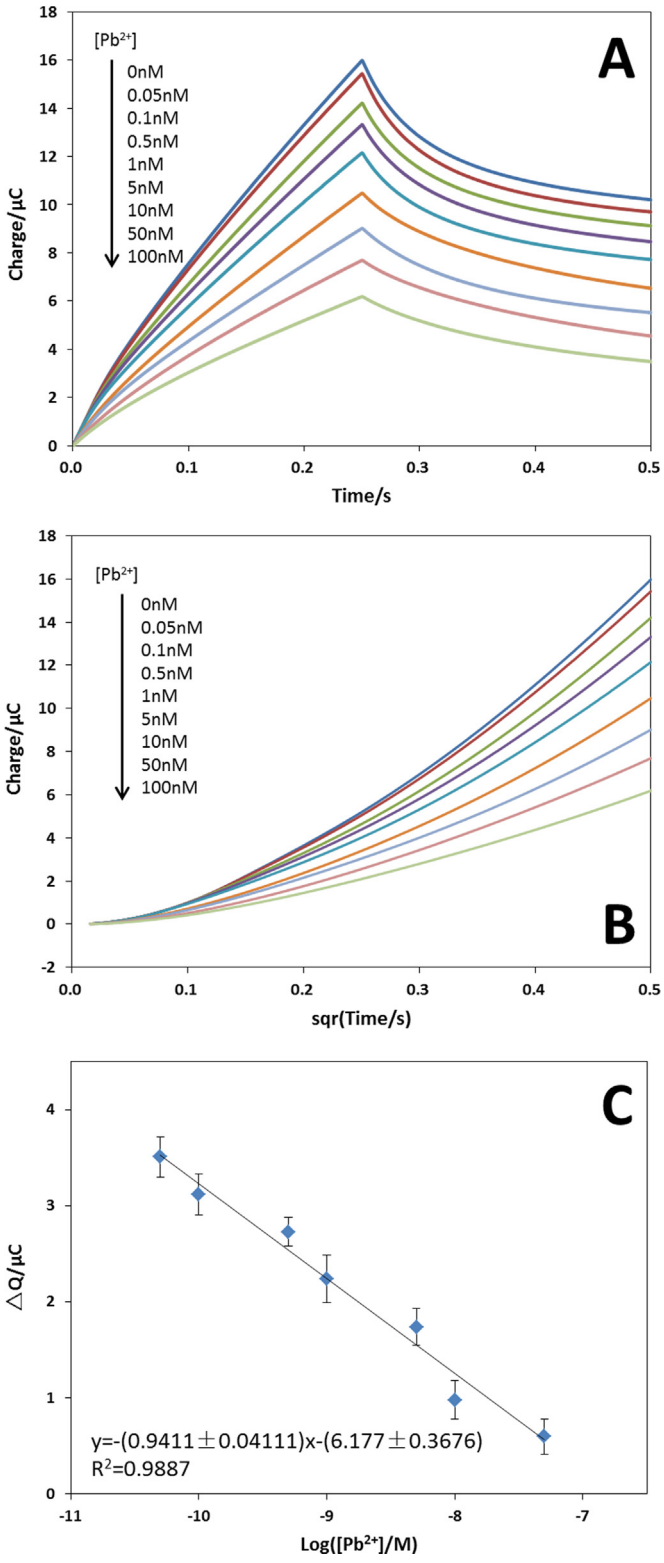

Fig. 3. Pb^{2+} target concentration-dependent curves for the chronocouloumetric aptasensor. (A) Representative chronocoulometric curves for NPG/GCE electrodes with Pb^{2+}-specific DNAzyme (P1) and substrate oligonucleotide (P2) in 10 mM Tris-acetate (pH 8.0) with 50 mM RuHex before and after reaction with Pb^{2+} at a series of concentrations (0.05, 0.1, 0.5, 1.0, 5.0, 10.0, 50.0 and 100.0 nM). Pulse period: 250 ms; pulse width: 700 mV. (B) The chronocoulometric curves are converted to Anson plots by plotting charge versus $t^{1/2}$. (C) Logarithmic plots for signal versus target Pb^{2+} concentration (0.05, 0.1, 0.5, 1.0, 5.0, 10.0, 50.0 and 100.0 nM) in the presence of NPG and AuNPs amplification. Signal was defined as the difference in the redox charge of RuHex after and before reaction with Pb^{2+}. Error bars stated the standard deviations of measurements taken from at least three independent experiments.

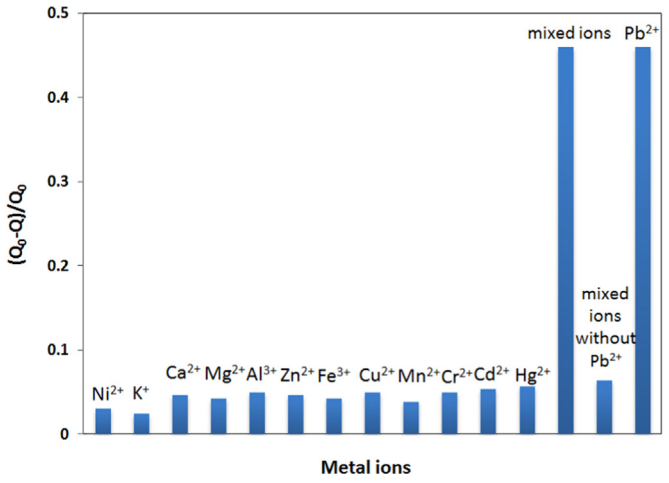

Fig. 4. Chronocoulometry signal in the presence of various metal ions. The concentration of each metal ion is 10 nM. The signal intensities were 5.75 C (buffer), 5.58 C (Ni^{2+}), 5.61 C (K^{+}), 5.48 C (Ca^{2+}), 5.50 C (Mg^{2+}), 5.46 C (Al^{3+}), 5.49 C (Zn^{2+}), 5.50 C (Fe^{3+}), 5.46 C (Cu^{2+}), 5.53 C (Mn^{2+}), 5.46 C (Cr^{2+}), 5.44 C (Cd^{2+}), 5.42 C (Hg^{2+}), 3.08 C (Pb^{2+}), 5.38 C (mixed ions without Pb^{2+}), and 3.13 C (mixed ions).

3.7. *Analysis of Pb^{2+} in water samples*

To test the practical application of the proposed method, several environmental water samples spiked with Pb^{2+}, with concentrations of 0, 5.0, and 10.0 nM, were tested using the proposed method and AFS. The environmental water samples used in the study were tap water, river water, and landfill leachate samples. All the samples were filtered through a 0.2 μm membrane and then centrifuged for 20 min at 12,000 rpm before the detection measurements were performed. The concentrations of total Pb^{2+} in water samples were measured to be less than 0.1 nM by AFS. The results were summarized in Table 1 and showed excellent agreement with the found values determined by AFS, suggesting good accuracy of the proposed method for Pb^{2+} detection in the water samples. Although the study here only demonstrated the detection of Pb^{2+} ions, the proposed sensing strategy can be applied to detecting different analytes (DNA or other metal ions) using other specificity structures that selectively bind the other analytes.

Table 1
Lead concentration in environmental sample determined by proposed method and AFS.

Sample	Added Pb^{2+} (nM)	Proposed method[a] (nM)	RSD[b] (%)	AFS[a] (nM)
Tap water 1	0	[c]	0	< 0.1
Tap water 2	5.0	5.07	2.42	5.03
Tap water 3	10.0	10.09	3.17	10.06
River water 1	0	[c]	0	< 0.1
River water 2	5.0	5.03	1.95	5.03
River water 3	10.0	9.98	2.76	10.07
Landfill leachate 1	0	[c]	0	< 0.1
Landfill leachate 2	5.0	5.05	3.29	5.08
Landfill leachate 3	10.0	10.1	2.85	10.06

[a] Mean of three replicate measurements.
[b] RSD = Relative signal deviation.
[c] No Pb^{2+} could be detected.

3.8. Reproducibility, stability and regeneration of the NPG-based biosensor

To further investigate the reproducibility of the proposed Pb^{2+} aptasensor, we repeatedly assayed the Pb^{2+} ions with three different levels under the same abovementioned procedures and conditions. Experimental results revealed that the Relative Standard Deviations (RSD) between five runs were 4.1%, 4.9% and 4.7% for 0.1 nM, 1.0 nM and 10 nM, respectively (Fig. S7A). The Pb^{2+} aptasensor was stored at 4 °C over 28 days, the electrochemical response did not change obviously (RSD 4.5%) for the detection of 1 nM Pb^{2+} solution (Fig. S7B).

In addition to sensitivity and selectivity, reusability is also an extremely important feature for aptasensors in the practical applications. The reusability was investigated as follows: the electrode could be regenerated by incubating the hybridization of P2 and P1-NPG modified electrode in hot water (90 °C) for 1 min, by which hybridized DNA was removed via thermal denaturation. After five cycles of regeneration procedure, the aptasensor almost retained its original hybridization efficiency, with the RSD of 4.6% at the same Pb^{2+} concentration of 1 nM (Fig. S7C). The low RSD represented that the developed strategy could be regenerated and used repeatedly.

4. Conclusion

In summary, a chronocoulometric aptasensor was constructed using DNAzyme modified with AuNPs, coupling with NPG modified electrode. The significant enhancement of 10.8-fold total active surface of NPG modified electrode was obtained, representing much more reaction sites of the Au-based 3D porous electrode, while DNA-AuNPs complexes provided a great number of sites for adsorption of RuHex molecules. The amplified detection strategy was introduced in detail, and produced an ultrasensitive electrochemical detection of Pb^{2+} down to nanomolar level with a relatively wide dynamic working linear range. It was also found that the aptasensor exhibited excellent selectivity, reproducibility, and could be easily regenerated. This simple aptasensor represented a promising potential for on-site detecting Pb^{2+} in drinking water.

Acknowledgments

This study was financially supported by the National Natural Science Foundation of China (51521006, 51378190, 51278176, 51408206, 51579098 and 51579096), the Program for New Century Excellent Talents in University (NCET-13-0186), Scientific Research Fund of Hunan Provincial Education Department (521293050), the Program for Changjiang Scholars and Innovative Research Team in University (IRT-13R17), the Fundamental Research Funds for the Central Universities, the Hunan Provincial Innovation Foundation for Postgraduate (CX2015B091), and the International S&T Cooperation Program of China (2015DFG92750).

Appendix A. Supplementary material

Supplementary data associated with this article can be found in the online version at doi:10.1016/j.bios.2016.02.053.

References

Aragay, G., Pino, F., Merkoci, A., 2012. Chem. Rev. 112 (10), 5317–5338.
Arduini, F., Calvo, J.Q., Amine, A., Palleschi, G., Moscone, D., 2010. Trac.-Trend. Anal. Chem. 29 (11), 1295–1304.
Baker, B.R., Lai, R.Y., Wood, M.S., Doctor, E.H., Heeger, A.J., Plaxco, K.W., 2006. J. Am. Chem. Soc. 128 (10), 3138–3139.
Brakmann, S., 2004. Angew. Chem. Int. Ed. 43 (43), 5730–5734.
Chen, A.C., Chatterjee, S., 2013. Chem. Soc. Rev. 42 (12), 5425–5438.
Chen, P., Greenberg, B., Taghavi, S., Romano, C., van der Lelie, D., He, C., 2005. Angew. Chem. Int. Ed. 117 (18), 2775–2779.
Ding, Y., Erlebacher, J., 2003. J. Am. Chem. Soc. 125 (26), 7772–7773.
Ding, Y., Kim, Y.J., Erlebacher, J., 2004. Adv. Mater. 16 (21), 1897–1900.
Dreaden, E.C., Alkilany, A.M., Huang, X.H., Murphy, C.J., El-Sayed, M.A., 2012. Chem. Soc. Rev. 41 (7), 2740–2779.
Erlebacher, J., Aziz, M.J., Karma, A., Dimitrov, N., Sieradzki, K., 2001. Nature 410 (6827), 450–453.
Fan, T., Liu, Y.G., Feng, B.Y., Zeng, G.M., Yang, C.P., Zhou, M., Zhou, H.Z., Tan, Z.F., Wang, X., 2008. J. Hazard. Mater. 160 (2-3), 655–661.
Feng, J.D., Zhao, W.J., Su, B., Wu, J.M., 2011. Biosens. Bioelectron. 30 (1), 21–27.
Ge, Y.Q., Wu, J., Ju, H.X., Wu, S., 2014. Talanta 120, 218–223.
Haiss, W., Thanh, N.T.K., Aveyard, J., Fernig, D.G., 2007. Anal. Chem. 79 (11), 4215–4221.
Hu, K.C., Lan, D.X., Li, X.M., Zhang, S.S., 2008. Anal. Chem. 80 (23), 9124–9130.
Huang, D.W., Niu, C.G., Wang, X.Y., Lv, X.X., Zeng, G.M., 2013a. Anal. Chem. 85 (2), 1164–1170.
Huang, D.L., Zeng, G.M., Feng, C.L., Hu, S., Jiang, X.Y., Tang, L., Su, F.F., Zhang, Y., Zeng, W., Liu, H.L., 2008. Environ. Sci. Technol. 42 (13), 4946–4951.
Huang, D.W., Niu, C.G., Ruan, M., Wang, X.Y., Zeng, G.M., Deng, C.H., 2013b. Environ. Sci. Technol. 47 (9), 4392–4398.
Jain, A.K., Gupta, V.K., Singh, L.P., Raisoni, J.R., 2006. Electrochim. Acta 51 (12), 2547–2553.
Ke, C.N., Hwang, C.I., Fan, C.P., 2003. IEEE. T. Consum. Electr. 49 (4), 983–989.
Lao, R.J., Song, S.P., Wu, H.P., Wang, L.H., Zhang, Z.Z., He, L., Fan, C.H., 2005. Anal. Chem. 77 (19), 6475–6480.
Levicky, R., Herne, T.M., Tarlov, M.J., Satija, S.K., 1998. J. Am. Chem. Soc. 120 (38), 9787–9792.
Liang, P., Sang, H.B., 2008. Anal. Biochem. 380 (1), 21–25.
Liu, J., Lu, Y., 2006. Nat. Protoc. 1 (1), 246–252.
Marbella, L., Serli-Mitasev, B., Basu, P., 2009. Angew. Chem. Int. Ed. 48 (22), 3996–3998.
Park, S., Chung, T.D., Kim, H.C., 2003. Anal. Chem. 75 (13), 3046–3049.
Qiu, H.J., Zhou, G.P., Ji, G.L., Zhang, Y., Huang, X.R., Ding, Y., 2009. Colloids Surf. B 69 (1), 105–108.
Quintana, J.C., Arduini, F., Amine, A., van Velzen, K., Palleschi, G., Moscone, D., 2012. Anal. Chim. Acta 736, 92–99.
Renner, R., 2004. Environ. Sci. Technol. 38 (12), 224A–227A.
Saha, K., Agasti, S.S., Kim, C., Li, X., Rotello, V.M., 2012. Chem. Rev. 112 (5), 2739–2779.
Shen, L., Chen, Z., Li, Y.H., He, S.L., Xie, S.B., Xu, X.D., Liang, Z.W., Meng, X., Li, Q., Zhu, Z.W., Li, M.X., Le, X.C., Shao, Y.H., 2008. Anal. Chem. 80 (16), 6323–6328.
Szamocki, R., Velichko, A., Holzapfel, C., Mucklich, F., Ravaine, S., Garrigue, P., Sojic, N., Hempelmann, R., Kuhn, A., 2007. Anal. Chem. 79 (2), 533–539.
Tang, L., Zeng, G.M., Shen, G.L., Li, Y.P., Zhang, Y., Huang, D.L., 2008. Environ. Sci. Technol. 42 (4), 1207–1212.
Taton, T.A., Mirkin, C.A., Letsinger, R.L., 2000. Science 289 (5485), 1757–1760.
Wang, Z.D., Lee, J.H., Lu, Y., 2008. Adv. Mater. 20 (17), 3263–3267.
Wu, L., Xiong, E.H., Zhang, X., Zhang, X.H., Chen, J.H., 2014. Nano Today 9 (2), 197–211.
Xiao, Y., Rowe, A.A., Plaxco, K.W., 2006. J. Am. Chem. Soc. 129 (2), 262–263.
Xu, C.X., Su, J.X., Xu, X.H., Liu, P.P., Zhao, H.J., Tian, F., Ding, Y., 2007. J. Am. Chem. Soc. 129 (1), 42–43.
Xu, P., Zeng, G.M., Huang, D.L., Feng, C.L., Hu, S., Zhao, M.H., Lai, C., Wei, Z., Huang, C., Xie, G.X., Liu, Z.F., 2012. Sci. Total. Environ. 424, 1–10.
Yang, X.R., Xu, J., Tang, X.M., Liu, H.X., Tian, D.B., 2010. Chem. Commun. 46 (18), 3107–3109.
Yola, M.L., Atar, N., Qureshi, M.S., Ustundag, Z., Solak, A.O., 2012. Sens. Actuators B 171, 1207–1215.
Zeng, G.M., Chen, M., Zeng, Z.T., 2013a. Science 340 (6139) 1403–1403.
Zeng, G.M., Chen, M., Zeng, Z.T., 2013b. Nature 499 (7457) 154–154.
Zhang, C., Liu, L., Zeng, G.M., Huang, D.L., Lai, C., Huang, C., Wei, Z., Li, N.J., Xu, P., Cheng, M., Li, F.L., He, X.X., Lai, M.Y., He, Y.B., 2014a. Biochem. Eng. J. 91, 149–156.
Zhang, C., Zeng, G.M., Huang, D.L., Lai, C., Huang, C., Li, N.J., Xu, P., Cheng, M., Zhou, Y. Y., Tang, W.W., He, X.X., 2014b. RSC Adv. 4 (98), 55511–55518.
Zhang, J.T., Li, C.M., 2012. Chem. Soc. Rev. 41 (21), 7016–7031.
Zhang, L., Chang, H.X., Hirata, A., Wu, H.K., Xue, Q.K., Chen, M.W., 2013. ACS Nano 7 (5), 4595–4600.
Zhang, Y., Zeng, G.M., Tang, L., Huang, D.L., Jiang, X.Y., Chen, Y.N., 2007. Biosens. Bioelectron. 22 (9–10), 2121–2126.
Zhou, Y.Y., Tang, L., Zeng, G.M., Zhang, C., Zhang, Y., Xie, X., 2016a. Sens. Actuators B 223, 280–294.
Zhou, Y.Y., Tang, L., Zeng, G.M., Chen, J., Cai, Y., Zhang, Y., Yang, G.D., Liu, Y.Y., Zhang, C., Tang, W.W., 2014a. Biosens. Bioelectron. 61, 519–525.
Zhou, Y.Y., Tang, L., Xie, X., Zeng, G.M., Wang, J.J., Deng, Y.C., Yang, G.D., Zhang, C., Zhang, Y., Chen, J., 2014b. Analyst 139 (24), 6529–6535.
Zhou, Y.Y., Tang, L., Zeng, G.M., Zhang, C., Xie, X., Liu, Y.Y., Wang, J.J., Tang, J., Zhang, Y., Deng, Y.C., 2016b. Talanta 146, 641–647.
Zhu, Y., Zeng, G.M., Zhang, Y., Tang, L., Chen, J., Cheng, M., Zhang, L.H., He, L., Guo, Y., He, X.X., Lai, M.Y., He, Y.B., 2014. Analyst 139 (19), 5014–5020.